



Effect of multiple climate change scenarios and predicted land-cover on soil erosion: a way forward for the better land management

Bilal Aslam · Umer Khalil · Maryam Saleem ·
Ahsen Maqsoom · Emadullah Khan

Received: 7 January 2021 / Accepted: 19 October 2021 / Published online: 28 October 2021
© The Author(s), under exclusive licence to Springer Nature Switzerland AG 2021

Abstract The ecosystem, biodiversity, and anthropological existence in the Chitral district are in danger due to the sediments and soil erosion stemming from the changes in the land-cover and climate. This research aims to practice the RUSLE model with the changes in the land-cover and climate in upcoming situations for 2030 and 2040 to evaluate soil erosion annually as per the spatial dissemination and the tendency of sediment yield. The multilayer perceptron (MLP), an artificial neural network (ANN), besides the Markov chain analysis was used to model upcoming land-cover. The Max Planck Institute model, which

demonstrated a revised bias as well as downscaled grid size under the Representative Concentration Pathways (RCPs), was used for examining the future changes in the climate. The modeled land-cover showed that the areas that are primarily comprised of natural trees and shrubs were transformed largely to agriculture and build-up areas. The average rainfall in the future under different RCP situations was elevated compared to the rainfall through historical time. The continuous variability in the R and C factors affects the probable soil erosion rate and sediment yield. Under RCP8.5 for both future years of 2030 and 2040, the extreme erosion rate was assessed at around 500 and 550 t/ha/year. Additionally, under the different RCP scenarios in 2030 and 2040, the outcomes of sediment yield were more significant than the sediment yield through historical time. The results showed that lower regions of the Chitral district are at risk of amplified soil erosion and sediment yield presently, as shown by the historical data and in the future. The produced soil erosion maps using ArcGIS 10.2 can play a valuable role in managing sustainable development, conservation of the watershed of the Chitral River, and reducing soil loss. Effective measures to overcome these concerns and mitigate the possible effects need to be planned and practiced, particularly the decrease in the storage volume of the reservoirs situated on the river.

B. Aslam (✉)
Department of Data Sciences, Riphah International
University, Islamabad, Pakistan
e-mail: bilalaslaml45@gmail.com

U. Khalil · A. Maqsoom
Department of Civil Engineering, COMSATS University
Islamabad, Wah Campus, Wah Cantt, Pakistan
e-mail: umerkhalil745@gmail.com

A. Maqsoom
e-mail: ahsen.maqsoom@ciitwah.edu.pk

M. Saleem
Department of Earth and Environmental Science, Bahria
University, Islamabad, Pakistan
e-mail: maryamsaleem17@gmail.com

E. Khan
Department of Geology, Abdul Wali Khan University,
Mardan, Pakistan
e-mail: emadgeo@awkum.edu.pk

Keywords Chitral district · Land-cover change ·
Soil erosion · Sediment yield · Climate change ·
RUSLE model

Introduction

Soil erosion is an utmost important ecological process that entails the separation, conveyance, and amassing of soil particles from a given preliminary region to a new depositional region (Gelagay & Minale, 2016; Polykretis et al., 2020). The soil particles present in the topmost layer of the land surface are moved from one place to another. Moreover, around the twentieth century, soil erosion, which is a continuing and intricate event, has been intensifying all across the world (Singh & Panda, 2017). The erosive agents, for instance, wind and water, are responsible for the transportation of the detached individual soil particles because of the erosion phenomenon from the soil mass (FAO, 2015). The present soil particles in the uppermost surface layer are moved from one field to another by erosion. The soil removed annually by water and wind is 75 billion metric tons, as demonstrated by the estimates (Diyabalanage et al., 2017). Furthermore, the worldwide soil erosion by water is 20–30 Gt year⁻¹ (gigatons per year) as indicated by FAO (FAO, 2015). Additionally, anthropological involvement has eroded 2 billion hectares globally. By this, the erosion because of water has counted to be 1100 million hectares (Ganasri & Ramesh, 2016).

The impacts of change in the climate also include the process of sedimentation and soil erosion as it will result in increased temperature and rainfall events, and the change in land-cover resulting from the actions of humans might cause the rising tendencies of soil erosion and sediment amount in a certain location (Chuenchum et al., 2020b). The Chitral river channel situated in the Chitral district may be endangered with the elevating tendencies of sediment amount and soil erosion owing to the upsurge in temperature, rainfall, and varying land-cover patterns resulting from anthropological actions. The Chitral River is among the key waterways that have impending challenges resulting from both the changing land-cover and climate, notably from the changing land-cover from the construction and development of hydropower. In the future, many areas of the Chitral district will be subjected to boosted soil erosion trends stemming from the variations in the land-cover and climate owing to the increased vulnerability of the soil structure to deforestation and land depreciation. The effectiveness of the hydraulic structures and the probable retaining capacity of

dams may be negatively affected due to the increased sediments (Eroğlu et al., 2010; Fu & He, 2007; Vaezi et al., 2017). Thus, there is a dire need to predict sediment yield as well as soil erosion resulting from the potential climate change combined with impending land-cover situations. These predictions will help in arranging countermeasures to alleviate the impacts on the Chitral River Basin.

For the assessment of soil erosion, the conventional field survey-based methods are time taking and costly. Thus, three different classes, for instance, empirical, conceptual, and physical, are used to categorize the several developed soil erosion models (Devatha et al., 2015). With the data utilized to operate the model, each model has its specific application scope (Rahman et al., 2009; Ricker et al., 2008; Wijesundara et al., 2018). Various studies concerning sediment and soil erosion problems in the sizeable catchments have employed these notions, for instance, empirical (Ferreira et al., 2015), conceptual (Schuol et al., 2008), and physical models (Nord & Esteves, 2005).

To speculate the extent of soil loss on an enduring basis in 1978, the United States Department of Agriculture (USDA) formulated an empirical soil erosion model named Universal Soil Loss Equation (USLE) (Abdo & Salloum, 2017). Later, the USLE model was revised as the Revised Universal Soil Loss Equation (RUSLE) or RUSLE model (Renard et al., 1997). For the estimation of sediment and soil erosion, the RUSLE model has been utilized widely (Hua-rong et al., 2006; Peng et al., 2007; Thuy & Lee, 2017; Yao et al., 2005; Zhou et al., 2014). The RUSLE model is interpreted among the widespread models owing to the reason that the diverse features of any significant river basin can be examined in the model with specific topographical tools (Kayet et al., 2018; Teng et al., 2018; Terranova et al., 2009). In curious sites, the sediment yield in terms of sediment erosion and deposition can be analyzed by modifying the RSULE model, as indicated by many current investigations (Chuenchum et al., 2020a; Kaffas et al., 2018; Rangsiwanichpong et al., 2018).

Moreover, in many regions, the land-cover dynamics affecting the hydrological conditions, rates of soil erosion, and greenhouse gas emissions have been investigated in preceding investigations on land-cover change exercising cellular automata, linear models, neural networks, regression analysis, agent-based

models, and Markov chain analysis (Guan et al., 2011; Guo et al., 2019; Mandle et al., 2017; Mas et al., 2014; Verburg et al., 2002). In order to model the upcoming land-cover as well as for the analysis of the variance among future land-cover besides the historical lands, the land-cover modeler (LCM) in TerrSet software is a suitable tool as indicated by most of the studies (Ansari & Golabi, 2019; Azimi Sardari et al., 2019; Kamwi et al., 2018).

Modeling the land-cover change, particularly the vegetation cover, for instance, the grassland, agricultural land, and the forest land, is really imperative because they are among the most influential factors influencing the process of soil erosion. Owing to the anthropological activities, the changes in land-cover change the rate of soil erosion. The LCM can be better used for modeling the forecast of the change in the land-cover for the upcoming period related to the criterion period (Anand et al., 2018; Olmedo et al., 2015).

For the assessment of the future climate trends in climate change investigations, generally, the global climate models (GCMs) have been utilized (Chuenchum et al., 2020b; Johnson et al., 2011). Nevertheless, the results of raw GCMs are required to be downscaled as per the grid size, plus with the historical period, the symmetrical error (biases) are required to be adjusted for carrying out the analysis related to the local climate as well as the additional hydrological functions (Hoang et al., 2016; Kiem et al., 2008; Mandle et al., 2017). It is suggested in most of the studies that investigators utilize GCMs that are entirely bias-corrected and downscaled from the accessible data resources of pertinent organizations and ventures, for instance, CORDEX, WorldClim, IMPAC-T, and CGIAR, to deliberate other apprehensions (Huang et al., 2014; Raghavan et al., 2018; Ruan et al., 2019).

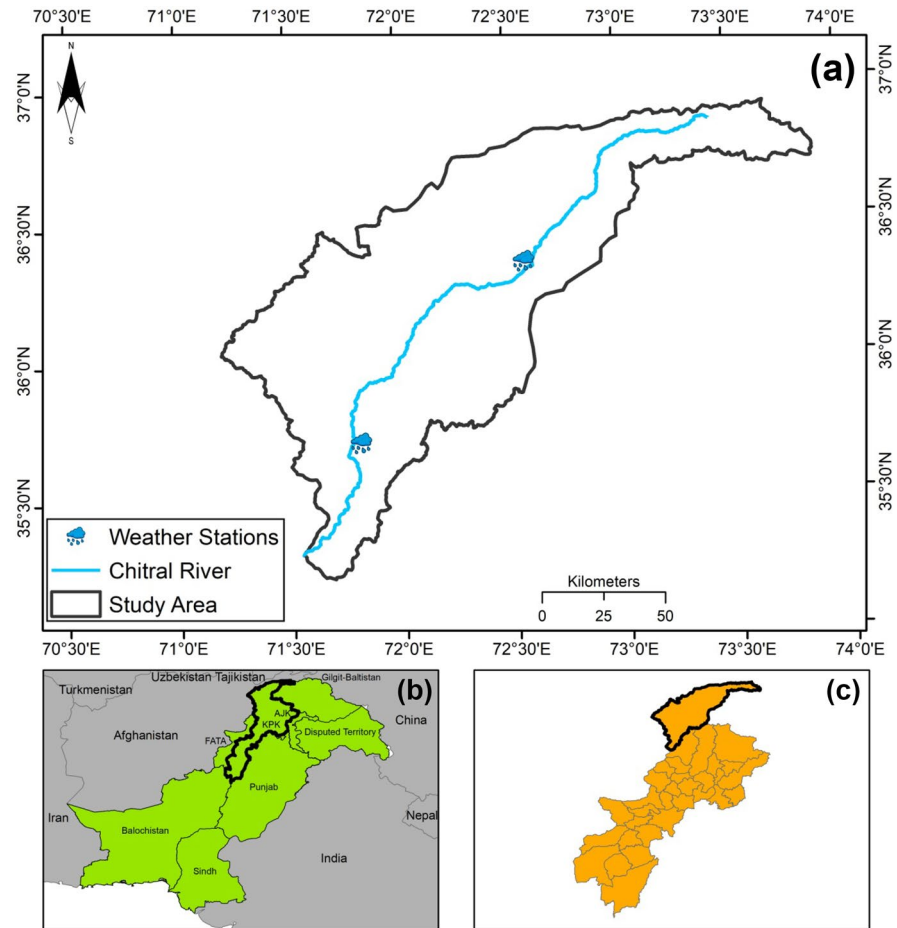
The aims of this research comprise the deliberation of the variations in the risks of sediment yield plus soil erosion in the years 2030 and 2040 by utilizing the RUSLE model combined with the geographical information system (GIS) along with remote sensing by considering the impacts of the potential climate change and impending land-cover circumstances. The ANN and Markov chain analysis in TerrSet software was used to investigate and model the alteration of future land-cover to evaluate the support practice factor (P) and cropping management factor (C) in 2030

and 2040. From the GCMs under RCP8.5 (pessimistic), RCP4.5 (intermediate), and RCP2.6 (optimistic), this study also deliberates the varying tendencies of impending rainfall and the rainfall erosivity factor (R). The policymakers and the concerned organizations can benefit from the fallouts of this research in selecting and implementing the appropriate strategies and actions for the viable advancement of the Chitral river basin.

Study area

Chitral District, situated in the north of Khyber Pakhtunkhwa province of Pakistan, is part of the Malakand division. With an area of 14,850 km² (5,730 sq mi), the Chitral district is situated in the extreme north of Pakistan. On the east side, the region of Gilgit Baltistan, on the west and north Nuristan, Badakshan, and Kunar provinces of Afghanistan, and on the south side, Dir and Swat districts of Khyber Pakhtunkhwa share their borders with the district. The Chitral city having geographical coordinates 35° 50' 46" N 71° 47' 09" E and with an area of 57 km² (22 sq mi) is the main city of the district, which sits on the west bank of the Chitral river. The Kūnar River, also recognized as the Chitral river in its upper reaches, is about 480 km long, situated in the eastern provinces (Nangarhar, Kunar, Nuristan) of Afghanistan and northern province (Khyber Pakhtunkhwa) of Pakistan. It appears just south of the Baroghil pass, near the border of Afghanistan in the upper part of the Chitral district. The melting snow and glaciers of the mountains of the Hindukush range feed the river. The Chitral river is at the base of the tallest summit of the Hindukush mountainous range, Tirich Mir.

Chitral district has more than 40 peaks of height greater than 6100 m and is counted as one of the most elevated regions of the world. The district has a very mountainous train, and Tirich Mir, with an elevation of 7708 m (25,289 ft), is the tallest summit of the Hindukush range. About 4.8% of the district area comprises forests, whereas 76% is composed of glaciers and mountains. Figure 1 illustrates the location of the study area in Pakistan's Khyber Pakhtunkhwa province. It also marks the presence of weather stations and the Chitral river in the Chitral district.

Fig. 1 Study area

Materials and method

RUSLE model

An empirical erosion model that has been employed in the computation as well as examination of the mean soil loss risk on land is the RUSLE model. It was established by the United States Department of Agriculture (USDA) from the Universal Soil Loss Equation (USLE). To better estimate the values of different parameters of the USLE, it was established in the late 1970s (Wischmeier & Smith, 1978). The RUSLE model, by integrating enhancements in the information probed by the USLE model, facilitates the evaluation of average soil loss per unit of area and, therefore, within the confines of a particular area, the evaluation of the spatial dissemination of soil erosion. Centered on the postulation that the separation and accumulation of the soil particles are governed by the

sediment carrying potential of the flow, the RUSLE model incorporates a collection of five parameters depicting the key factors of water-simulated soil erosion. Either the RUSLE method can be practiced on statistical and empirical data by utilizing the GIS methods, or it can be executed centered on the literature values (Fu et al., 2005; Karaburun, 2009; Lufafa et al., 2003). The outcomes are consistent concerning the evaluation of the consequences of erosion induced by water (Ozcan et al., 2008). It is centered on an empirical equation that can be certainly devised in a GIS framework (Renard et al., 1997). The subsequent comparison presents the RUSLE model:

$$A = R \times K \times LS \times C \times P \quad (1)$$

where A is the average soil erosion in $t \text{ ha}^{-1} \text{ year}^{-1}$, R is the rainfall erosivity factor measured in $\text{MJ mm ha}^{-1} \text{ h}^{-1} \text{ year}^{-1}$, K is the soil erodibility factor measured in $t \text{ ha MJ}^{-1} \text{ mm}^{-1}$, LS is the slope length and

steepness factor having no dimensions, C is the cover management factor with no dimensions, and P is the support practice factor also having no dimensions.

The climate change scenarios and rainfall erosivity factor

For studying the soil erosion problems, an important factor to consider is the rainfall erosivity (R) factor. The intensity and inconsistency of rainfall are considerably influenced because of climate change, as has been indicated by most of the studies (Chuenchum et al., 2020b; Moss et al., 2010). Among the international research groups globally, the platform for simulated collaboration is the current Coupled Model Intercomparison Project Phase 5 (CMIP5) (Mehran et al., 2014; Taylor et al., 2012), under which the GCMs have been applied extensively. For the consideration of the impending climate events, this step is carried out. Relying on the statistical models and other associated expressions, the association among the ocean and the planetary atmosphere has been used for the development of the GCMs. For the comprehension and the prediction of climate change, the Earth’s ocean and atmosphere processes were modeled.

The CGIAR Research Program on Climate Change, Agriculture, and Food Security was utilized to download the CM rainfall dataset under CMIP5 (<http://www.ccafs-climate.org/>). Under the Earth System Grid online platform globally, such an organization delivers upcoming climate data in GCMs from the 2020s to the 2080s. Owing to the spatial resolution restriction in GCMs, the dataset demonstrated corrected the symmetrical error (biases), and therefore by utilizing the delta change technique, the dataset was downscaled at an elevated spatial resolution of 1 km. For the analysis of the hydrological modeling and the catchment scale, this method is extensively utilized for the GCM output (Navarro-Racines et al., 2020; Navarro-Racines & Tarapues, 2015; Ramirez-Villegas & Jarvis, 2010).

For the investigation of the sediment yield and soil erosion, centered on the former investigations and the literature, we opted for a suitable GCM model in the Chitral district. The MPI-ESM-LR, established by the Max Planck Institute (MPI) (Giorgetta et al., 2013), was considered as suitable to be used for climate forecasting in terms of the scale and time on a global level, as affirmed

by most of the studies concerning the climate change analysis (Chhin & Yoden, 2018; Ruangrassamee et al., 2015; Tangang et al., 2019). For three different situations of greenhouse gas discharges, comprising RCP8.5 (pessimistic), RCP4.5 (intermediate), and RCP2.6 (optimistic), the impending rainfall data from 2020 to 2030 besides 2020 to 2040 were modeled. Under the IPCC, the Representative Concentration Pathway (RCP) concept was used to determine these situations.

As vast long-term data is not existing, thus, analytical computation of the R factor is not possible. Consequently, by using the existing rainfall data, the R factor is calculated by using the other techniques (Efthimiou et al., 2014). The most commonly practiced empirical technique, Modified Fournier Index (MFI), was utilized in this research. The study conducted by Aslam et al. (2020) also applied this calculation for the R factor, which is demonstrated by the following equation:

$$MFI = \sum_{j=2}^{12} \frac{p_i^2}{P} \tag{2}$$

where *P* is the yearly rainfall in mm, and *p_i* is the monthly rainfall for the *i*-month in mm. There is a strong linear correlation among the MFI and the R factor of the RUSLE model (Ganasri & Ramesh, 2016). This method was proposed by Licznar (2004), who calculated the R factor by using a previous rainfall database from 4 stations in Poland. The established power-type relation of yearly R factor against the MFI values having a correlation coefficient as *r*=0.64 was as follows:

$$R = 0.2265 \times MFI^{1.2876} \tag{3}$$

Soil erodibility and topographic factor

The tangible soil characteristics in the Chitral river basin were based to establish the soil erodibility (K) factor. The K factor was analyzed by applying the soil data obtained from the satellite data. We used the soil texture map of the Chitral district, and the values to different classes of soil type were assigned according to preceding studies (Aslam et al., 2020; Maqsoom et al., 2020; Sharma et al., 2011; Ullah et al., 2018).

The topographic factor (LS) is a sequence of two slope properties: the slope length (L) and steepness (S). Both of the mentioned factors embody the impact of the topography of a region on the process

of soil erosion. The present study utilized the DEM data having 30 m spatial resolution which was downloaded from the Shuttle Radar Topography Mission (SRTM) and then processed in ArcGIS 10.2 software. The equation recommended by Mitsova et al. (1999) was used in this research for the computation of the LS factor, which is as follows:

$$LS = (m + 1) [A_s / 22.13]^m [\sin b / 0.0896]^n \quad (4)$$

where A_s is the up-slope contributing area per unit width in meters, and b is the slope angle in radians, whereas m (0.4 to 0.6) and n (1.0 to 1.4) are parameters. Exponents m and n ought to be adjusted for a certain prevalent type of flow and soil conditions if the data are available. For the computation of the LS factor, the ArcMap GIS 10.2 software was used.

$$LS = \text{power}(\text{flowaccumulation} * \text{cellsize} / 22.13, 0.6) * \text{Power}(\sin(\text{slope}) * 0.01745) / 0.0896, 1.3) \quad (5)$$

Cropping management and support practice factors

The support practice (P) factor was ascertained, and the cropping management (C) factor was determined. The influence of land-cover on soil erosion, mainly water erosion, is indicated by the P factor. This factor explains the altering of possible erosion by running water, for instance, buffer strips, contouring, terraced contour farming, and minimum tillage. Later, to the modeling of the C factor, the P factor was stipulated. In the present research, the deliberation of the P factor is centered on the investigation conducted by Yang et al. (2003) that established the categorization of the C factor as per the land-cover to be the P factor owing to the constraints in the field observations in the Chitral district (Table 1).

Modeling of the change in the land-cover

For the development of land and decision support system, among different modules, the LCM module is the most widely used, which is incorporated completely into the TerrSet software formulated by Clark Labs of the Clark University. Additionally, the mentioned software can model with the IDRISI software as well as the ArcGIS extension (Nor et al., 2017).

Utilizing the empirical model associations to illustrative variables such as closeness to roads and slope, the LCM can evaluate the current and impending changes in land-cover besides their repercussions and model the upcoming changing land-cover situations (Pérez-Vega et al., 2012). Three different process categories can be specified for the modeled process in the LCM module such as change analysis, which involves the analyzation of the former change in the land-cover, change potentials, which includes the modeling of the possibility for land changes, and change projection that comprises the prediction of the progression of change through the upcoming times. These different operating practices are centered on past land change from a specified time to probable upcoming land situations.

For the analysis of the prediction and monitoring of land-cover, there is a need to apprehend the modeled process in the LCM module and TerrSet software. The primary step of the model is the analysis of the change that is required to be evaluated for contemplating the variance among land-cover maps in 2000, 2010, and 2020. The illustrative variables, for instance, slope, closeness to the road, and elevation, are based for modeling the change from one land-cover to another. The variance in land-cover can be recognized as the alterations from one land-cover scenario to another over time. Increasing population, expanding build-up area, and the increasing demand for natural resources are consequential for the changing land-cover. The next stage is the evolution possibilities directed to the artificial neural network, an MLP neural network. At this stage, for producing the possible change maps suitable for each change in the structure of the sub-model, the change variables are selected by using the MLP neural network

Table 1 Classification of the land-cover as per C and P factor

Land-cover of the Chitral district	C factor (FAO, 2000)	P factor (Yang et al., 2003)
Agriculture	0.5	0.5
Bare Areas	0.35	1
Build-up	0.1	1
Natural Shrubs	0.2	1
Natural Trees	0.001	1
Snow	0.001	1

(Rumelhart et al., 1985). For improving the accuracy, each of the changes will be altered by reducing the RMSE error. The resulting fallouts of this stage were the possible change maps of each conceivable change.

In the LCM module, the forecasting of the change is the concluding stage. The LCM can forecast an upcoming scenario for a certain upcoming date by utilizing the past changing rates and the possible change models. The incentives, constraints, and influential variables to the upcoming variations, for instance, organized infrastructural alterations and zoning maps, among time phases *i* and *j* will be defined by the change prediction; such process then will use Markov chain analysis to compute the relative extent of change to the impending date (Norris, 1998). For the evaluation and the detection of land-cover change in this study, we used the land-cover data acquired from the LANDSAT 8 satellite with a spatial resolution of 1 km in the Chitral district for 2000, 2010, 2015, and 2020. However, to observe the land change in each area utilizing the ArcGIS 10.2 extension, the arrangement of land-cover maps from every single state should be altered. Following the new categorization in the LCM assessment, the six land-cover classes are agriculture, bare areas, build-up, natural shrubs, natural trees, and snow. Centered on the MLP neural network, the LCM module, the TerrSet software, and the Markov chain analysis were operated to deliberate the past change in the land-cover and forecast the upcoming land-cover maps. This research aims to predict upcoming land-cover for the years 2030 and 2040, relying on past land-cover maps in the years 2000, 2010, and 2020.

For the analysis of the sub-models of the change possibilities by utilizing the MLP neural network, the six change sub-models, namely agriculture to build-up, agriculture to bare areas, natural shrubs to agriculture, natural trees to agriculture, natural trees to build-up, and bare areas to agriculture, were established and entered into the LCM module. Six explanatory variables, namely distance from urban areas, distance from river, distance from roads, slope, aspect, and elevation, were also included in land-cover change analysis. The considered illustrative variables have been utilized to contemplate the modeling concerning the change in land-cover as affirmed by most of the studies.

Evaluation of land-cover change models

For the assessment of the accuracy of land-cover change models, the criterion land-cover maps utilizing three Kappa indexes through the operation of TerrSet software were used for the calibration and verification of the modeled outcome of the impending land-cover map. The employed Kappa indexes are Kappa for quantity and location (K_{location} & $K_{\text{location strata}}$), Kappa for no ability (K_{no}), and the traditional Kappa index (K_{standard}). The consistency among two distribution of class sizes and two categorical datasets is shown by the K_{no} and the K_{standard} respectively by utilizing a stochastic model of arbitrary distribution of class changes comparative to the preliminary map (van Vliet et al., 2011). The understanding of the various precisions as per the quantity and location is presented by the K_{location} and $K_{\text{location strata}}$. The following equations represent the K_{standard} , K_{no} , and K_{location} and $K_{\text{location strata}}$, respectively:

$$K_{\text{standard}} = \frac{p_o - p_e}{1 - p_e} \tag{6}$$

$$K_{\text{no}} = \frac{p_{\text{max}} - p_e}{1 - p_e} \tag{7}$$

$$K_{\text{location}} \ \& \ K_{\text{location strata}} = \frac{p_o - p_e}{p_{\text{max}} - p_e} \tag{8}$$

where:

- p_o represents the noted fraction of agreement.
- p_e signifies the anticipated fraction of agreement.
- p_{max} embodies the extreme fraction of agreement.

For the Kappa index, the extreme value is generally fixed to 1. Less matching is also indicated by the decreasing Kappa index. Therefore, if there is a consistency in the Kappa index values, it indicates that the modeled land-cover map can be utilized in the analysis. Sequentially, the C factor is established with our outcomes of the projected land-cover map by utilizing the data from FAO (2000).

Deliberation of the important factors in the RUSLE model

The following two equations were used primarily to obtain the logarithmic forms of all the input factors in the RUSLE model:

$$\ln(A) = \ln(R \times K \times LS \times C \times P) \quad (9)$$

$$\ln(A) = \ln(R) + \ln(K) + \ln(LS) + \ln(C) + \ln(P) \quad (10)$$

where $\ln(A)$ signifies the rate of soil erosion in the logarithmic association and $\ln(R, K, LS, C, \text{ and } P)$ signifies the values of the input factors in the RUSLE model as per the logarithmic form. After this conversion, the multiple linear regression was utilized for the assessment of the influencing factors on the soil erosion process by considering the upcoming land and climate change situations in the intended area. The following equation shows the multiple linear regression:

$$\ln(A) = \beta_0 + \beta_i \ln(R) + \beta_j \ln(K) + \beta_k \ln(LS) + \beta_l \ln(C) + \beta_m \ln(P) \quad (11)$$

where the standard coefficient (β) in the above equation can signify the distinct units of the input factors, β_0 represents the intercept of soil erosion rate (constant values), and β_{i-m} is the coefficient of regression of every single illustrative variable from evaluation. The statistical outcomes from the preceding model were analyzed by utilizing the SPSS software. In this research, the determined statistical significance level was 95%.

The RUSLE model for the evaluation of sediment yield

Initially, the original USLE model was employed for the analysis of soil erosion; then, all the factors were introduced into the RUSLE model. The estimation of the yearly soil erosion can be transformed into the sediment yield by this method centered on the input RUSLE factors. The deliberation of sediment yield of the RUSLE model involving the changes in the land-cover and climate under the upcoming scenarios of years 2030 and 2040 was estimated. The technique which was practiced for the estimation of the sediment yield in the present study was also used by Ullah et al. (2018) for the assessment of sediment yield in the Potohar region of Punjab province, Pakistan. In the Chitral district, the same technique has also been practiced by Maqsoom et al. (2020) to evaluate the sediment yield.

The sediment delivery ratio (SDR) was computed through disseminating sediment yield by the drainage area of the watershed.

Consequently:

$$SDR = \frac{Y}{A} \quad (12)$$

or else:

$$Y = SDR \times A \quad (13)$$

where “Y” is the sediment yield, and “A” is the drainage area. The outcomes from this approach can be exhibited as the spatial dissemination of the sediment deposition or yield capacity and soil erosion.

Results

Climate change scenario

For different RCP scenarios, the future rainfall in 2030 and 2040 is shown in Fig. 2. The extreme values of rainfall were positioned primarily in the southwestern region of the Chitral district, as demonstrated in Fig. 2. The comparison among the monthly average rainfall from the historical period and the monthly average future rainfall under the different RCP scenarios in 2030 and 2040 for the Chitral district is displayed in Fig. 3. Similar rainfall patterns were observed for the future (in 2030 and 2040) for the different RCP scenarios, but the future rainfalls were different regarding their magnitude plus the highest rainfall in all the months, as indicated by the outcomes. The maximum and minimum rainfalls from 2000 to 2020 were 95 and 5 mm, respectively, whereas the average monthly rainfall in the historical period was 34.33 mm. Under the different RCP scenarios (RCP2.6, RCP4.5, and RCP8.5) in 2030 and 2040, the mean values of future rainfalls were 37.33, 39.33, and 38.33 mm and 39.33, 41.33, and 40.33 mm, respectively. However, under different RCP scenarios for both 2030 and 2040, the spatial dissemination of the R factor is exhibited in Fig. 4. The R factor under different RCP scenarios varied in 2030 from 2.52 to 1749.73 MJ mm ha⁻¹ h⁻¹ year⁻¹ and in 2040 from 81.59 to 1758.5 MJ mm ha⁻¹ h⁻¹ year⁻¹, respectively.

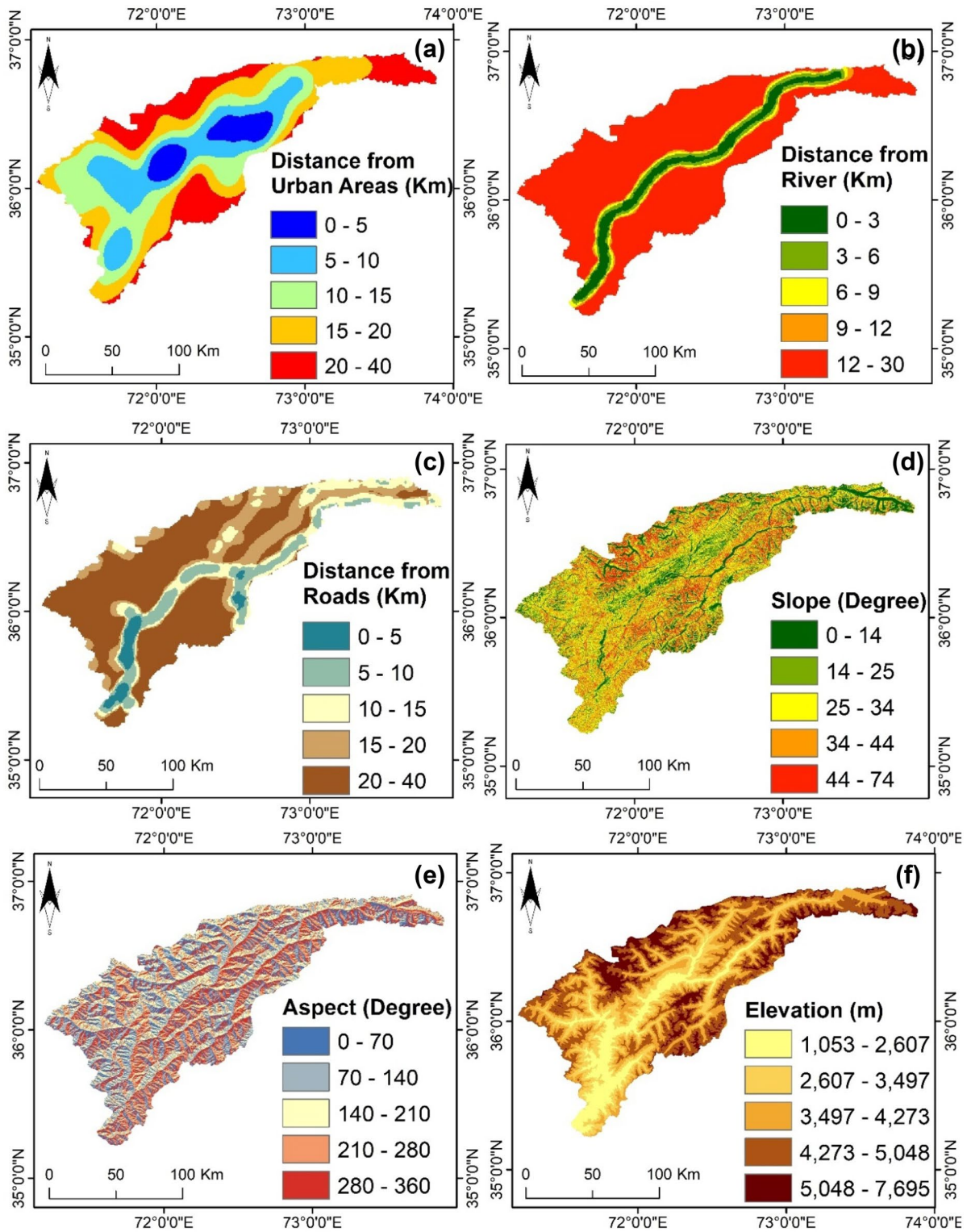


Fig. 2 Future rainfall of the study area in 2030 and 2040 under different RCP scenarios

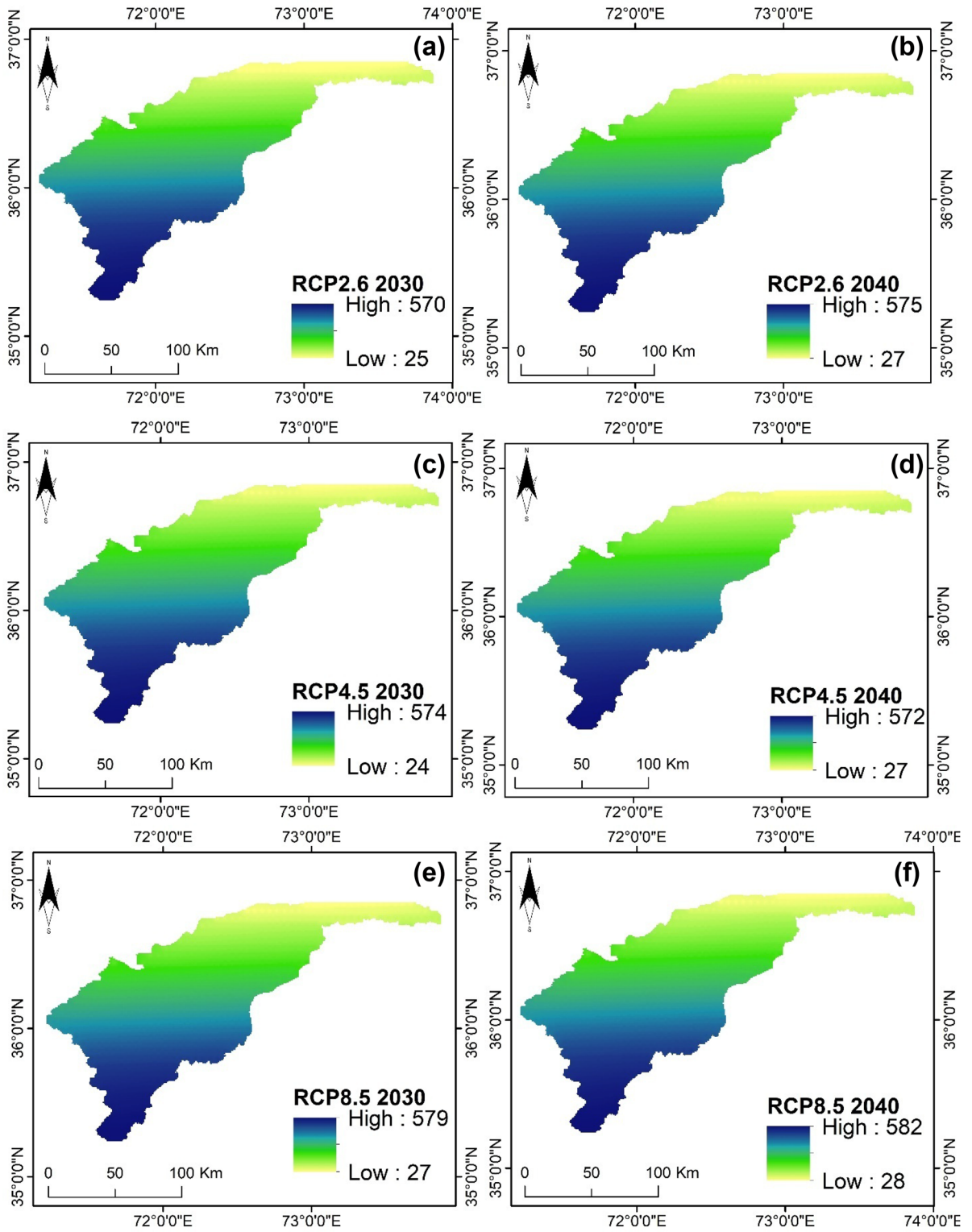


Fig. 3 Historical rainfall vs future rainfall of the study area in 2030 and 2040

Previous and future land-cover change

The changes resulted due to the socio-economic development (the upsurge in population and human activities) through the course of time are presented by the land-cover maps in 2000, 2010, 2015, and 2020 as portrayed in Fig. 5. For LCM modeling, the criterion was the land-cover map in 2000, which is covered mainly by the natural shrubs (39%), followed by the snow (36%), natural trees (8%), bare areas (8%), the build-up (7%), and agriculture (2%) as evident from Table 2.

The map of the six descriptive variables used for modeling the change maps in the LCM module is shown in Fig. 6a–f. The map of the variable distance from urban areas is shown in Fig. 6a. The map was divided into five classes based on the distance from the urban area ranging from 0 to 40 km. The farthest distance class was 20 to 40 km and is exhibited by the red color on the map. For the variable of distance from the river, the map is presented in Fig. 6b. The entire Chitral district was divided into five classes centered on the distance from the river ranging from 0 to 30 km. The Chitral River is the main river in the area that passes through the central region. The nearest areas are highlighted by the green color and the remotest areas by the red color. The map of the variable distance from roads is shown in Fig. 6c. Similarly,

the whole area was divided into five classes ranging from 0 to 40 km. Blue and brown colors, respectively, illustrate the nearest and the remotest areas on the map.

Furthermore, Fig. 6d exhibits the map of slope for the study area. The entire area was divided among five classes ranging from 0° to 74°. The steepest slopes are represented by the red color in the map and are particularly located in the peripheral regions of the Chitral district. Next, the aspect map of the district is shown in Fig. 6e, which is also divided into five classes varying in the range of degrees. The aspect map ranges from 0° to 360°. The aspect of the slope shows the position of the slope towards the sunlight and wind. Lastly, the map of the elevation is presented in Fig. 6f. The elevation in the district ranges from 1053 to 7695 m and is divided into five classes to locate the high elevation areas. The high elevation areas are represented by brown color in the map and are primarily found in the peripheral regions of the Chitral district.

For the modeling of possible change, the assessment outcomes of the MLP neural network comprising the values of accuracy percentage, training RMSE, and the testing RMSE are illustrated in Table 3. High accuracy, thus reliability, was exhibited by all the six sub-models that was ranging from 71.89 to 86.63%.

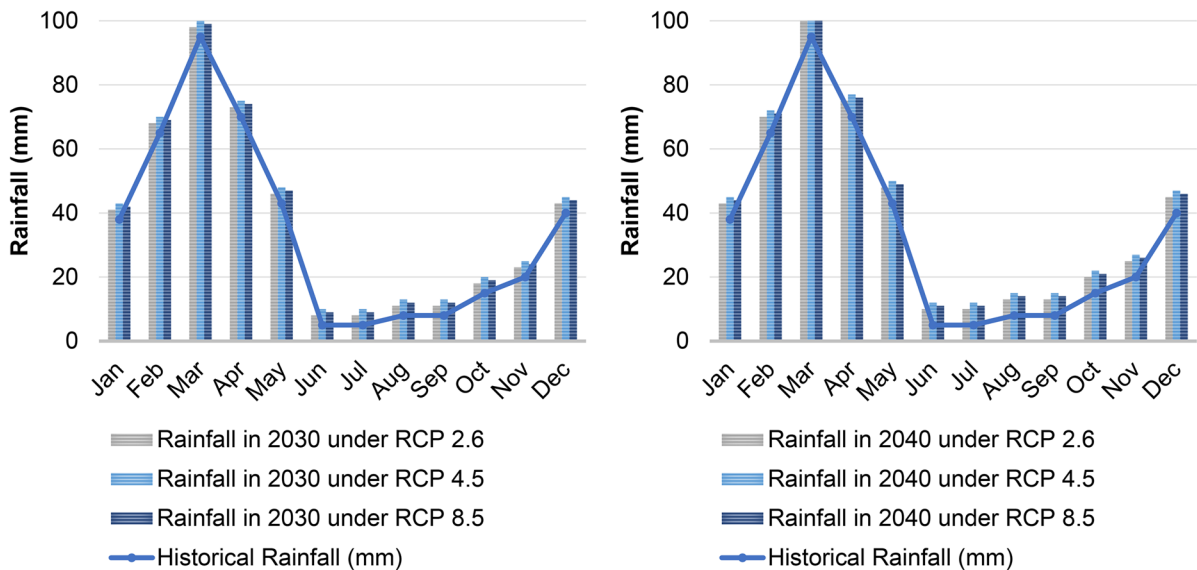


Fig. 4 R factor of the study area in 2030 and 2040 under different RCP scenarios

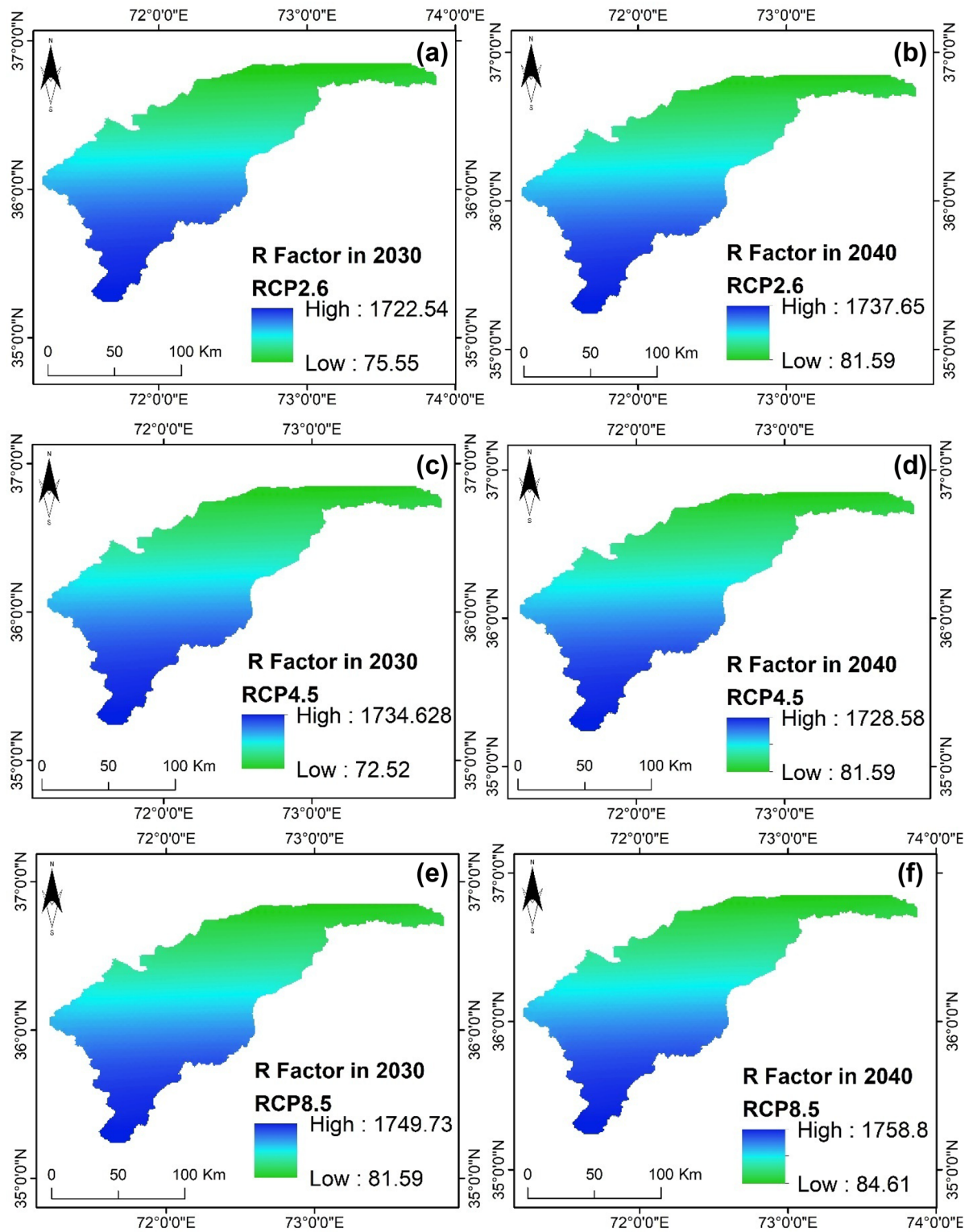


Fig. 5 Land-cover of the study area in 2000 a, 2010 b, 2015 c, and 2020 d, and the modeled land-cover in 2030 e and 2040 f

Table 2 Description of change in land-cover through 2000, 2010, 2020, 2030, and 2040

Land-cover	2000		2010		2020		2030		2040	
	Area (ha)	Area (%)	Area (ha)	Area (%)	Area (ha)	Area (%)	Area (ha)	Area (%)	Area (ha)	Area (%)
Agriculture	28,982.4	2	43,473.6	3	90,342.4	6	115,929.7	8	159,403.3	11
Bare areas	115,929.7	8	130,420.9	9	161,054	11	173,894.5	12	188,385.7	13
Build-up	101,438.1	7	115,929.7	8	136,539	9	159,403.3	11	202,876.9	14
Natural shrubs	565,157.2	39	550,665.9	38	515,637.5	36	492,701	34	449,227.4	31
Natural trees	115,929.7	8	101,438.4	7	80,471.7	6	72,456.04	5	57,964.83	4
Snow	521,683.6	36	507,192.2	35	465,076.1	32	434,736.2	30	391,262.6	27

Land-cover prediction through LCM

The possibility of change matrix from 2000 to 2020 is shown in Table 4. The greatest change was the change of bare areas to the agricultural area, whereas the possibility of the lowest change was the change of the area covered by natural trees to the agricultural area to model the land-cover prediction, as shown in Table 4.

The predicted land-cover maps in 2020, 2030, and 2040 are also presented in Fig. 5. The observed values of utilized four kappa statistics, namely $K_{standard}$, K_{no} , and $K_{location}$ and $K_{location strata}$ for checking the accuracy of the cell of predicted maps, were 0.948, 0.893, and 0.963, respectively.

Soil erosion assessment utilizing the RUSLE model

The value of the C factor in 2030 and 2040, as exhibited in Fig. 7, extends from 0 to 1, and has a mean value of 0.5. The outcomes showed that the central part of the Chitral district has more agricultural areas as compared to the remaining area. The regions in red color in the figure indicate that they comparatively have a high C factor value. In comparison, most of the southwestern region of the study area is comprised of natural trees and shrubs, which exhibited comparatively have low C factor values. However, in this study, both in 2030 and 2040, the K and LS factors are persistent for all the scenarios. The value of the K factor was varying from 0.1 to 0.4 t ha MJ⁻¹ mm⁻¹, as exhibited in Fig. 7. The elevation of the study area accounts for the values of the K factor. Those areas with low elevation showed low K values, whereas the high elevation area showed high K values. The LS factor was ranging from 0.2 to 6.3, as shown in Fig. 7. Most areas in the Chitral district have

moderate to higher steep and fleeting slopes. Hence, comparatively high LS values can be seen to be pointed out in the central regions of the study area, whereas comparatively low LS values were scattered all across the study area.

The achieved prediction outcomes of the soil erosion through the RUSLE model can be split among two situations in the upcoming times, comprising the soil erosion in 2030 as well as in 2040, as shown in Fig. 8. The first situation illustrates that the average soil erosion rates of different RCP scenarios, such as RCP2.6, RCP4.5, and RCP8.5 in 2030, were 240, 250, and 265 t/ha/year, respectively. Whereas the second situation shows that in 2040, the mean soil erosion rates were 250, 257.7, and 290 t/ha/year for the different RCP scenarios, for instance, RCP2.6, RCP4.5, plus RCP8.5, correspondingly. Under all the RCP scenarios, both situations of soil erosion in 2030 and 2040 showed that the eroding agents extremely eroded most regions in the lower part of the Chitral district. In contrast, the upper parts of the district experienced the most moderate and high erosion.

Evaluation of the correlation among the RUSLE input factors and the soil erosion rate

Table 5 indicates the outcomes of the correlation analysis that was performed among the RUSLE input factors and the soil erosion rate. A solid relationship is signified by all the standardized coefficients of the input factors with the RUSLE input factors of the soil erosion rate (Table 5), and they can be replaced in Eq. (5). Owing to the blunt change in the land-cover corresponding to the socio-economic growth, for the soil erosion, the C factor in the Chitral district was a strong influencing factor as it can be comprehended from the results.

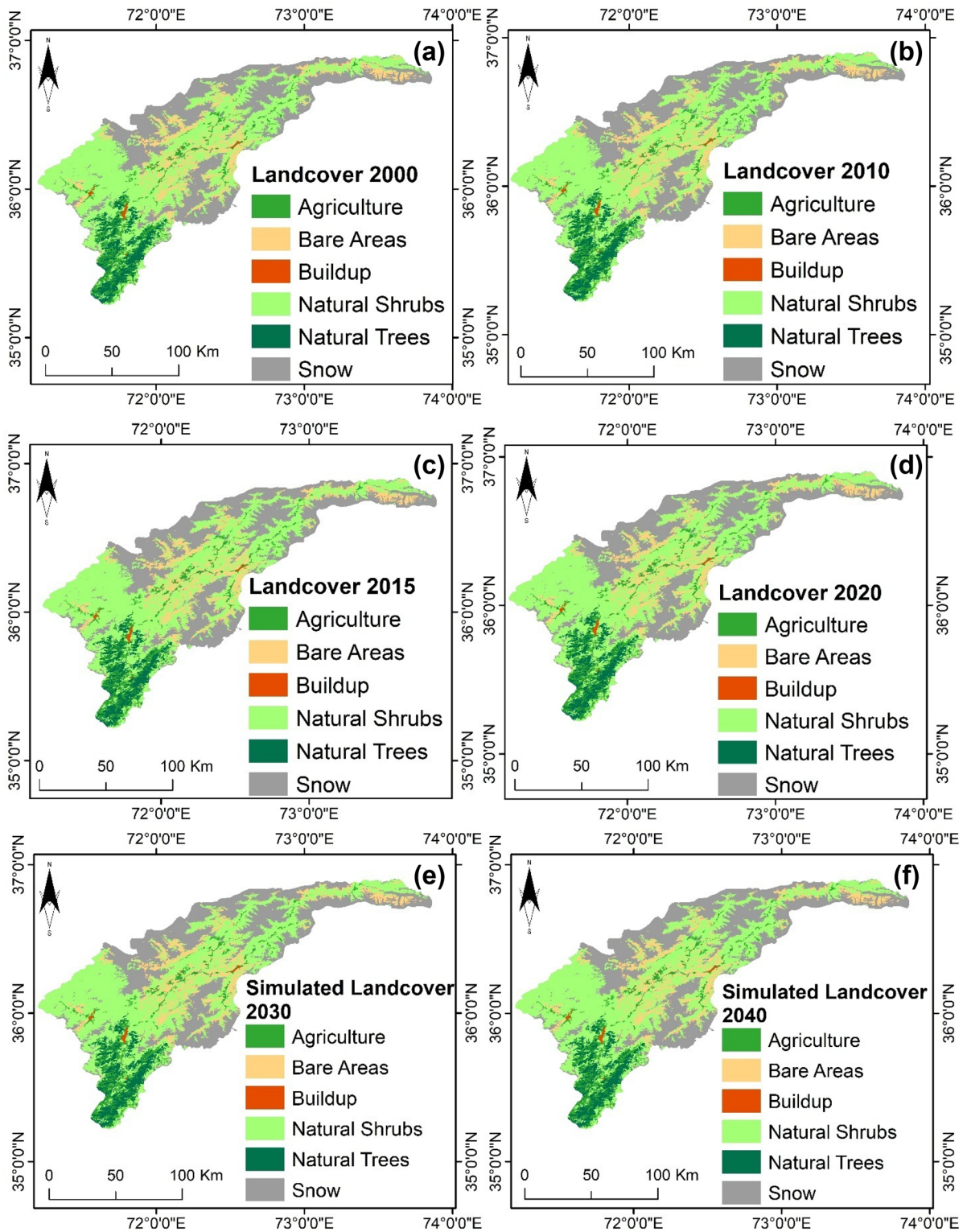


Fig. 6 Six explanatory variables including distance from urban areas **a**, distance from river **b**, distance from roads **c**, slope **d**, aspect **e**, and elevation **f**

Table 3 Valuation of all sub-models by utilizing the MLP neural network in change

Sub-model	Accuracy (%)	Training RMSE	Testing RMSE
Agriculture to build-up	82.45	0.002	0.0022
Agriculture to bare areas	84.68	0.0018	0.002
Natural shrubs to agriculture	79.58	0.0021	0.0023
Natural trees to agriculture	71.89	0.0024	0.0026
Natural trees to build-up	85.96	0.0018	0.002
Bare areas to agriculture	86.63	0.0017	0.0019

Evaluation of sediment yield utilizing the RUSLE model

In each grid cell of the study area, the modeled outcomes of sediment deposition and erosion for all the RCP scenarios in 2030 and 2040 are displayed in Fig. 9. Under all the RCP scenarios, for both 2030 and 2040, the impending sediment deposition and erosion range from <80 to >200 t/ha/year. In the central and particularly in the lower regions of the Chitral district, relatively high sediment erosion occurs, as can be seen from all the sediment deposition and erosion maps. The northwestern and predominantly the central part of the district have moderate to high sediment erosion, as shown in Fig. 9. Whereas in most of the peripheral regions of the study area, the relatively low sediment deposition was noticed.

The sediment deposition and erosion in the area for different RCP scenarios in 2030 and 2040 were categorized in five different classes ranging from low to high in terms of t/ha/year, as exhibited in Table 6. The percentages of the area under these different severity classes were also computed. In 2030, under all the three RCP scenarios, the maximum portion of the Chitral district lies in the least severity class of sediment deposition and erosion, having a value <80 t/ha/year, and the percentages were 36%, 33%, and 31%, respectively. Meanwhile, the maximum area percentages in 2040 were 34%, 29%, and 27%, and they also fall in the low severity class.

Table 4 Possibility of change matrix from 2000 to 2020

	Agriculture	Bare areas	Build-up	Natural shrubs	Natural trees	Snow
Agriculture	0.985	0.007	0.008	0	0	0
Bare areas	0	0.987	0.007	0.006	0	0
Build-up	0	0	1	0	0	0
Natural shrubs	0.04	0.001	0.02	0.939	0	0
Natural trees	0.05	0	0.02	0	0.931	0
Snow	0	0	0	0.005	0.01	0.985

Discussion

Among the most severe natural threats across the globe, soil erosion owing to the harsh economic and environmental impacts instigated by the stages of sedimentation and soil loss has been addressed as one. The sustenance of human beings is facing severe threats due to the continuous effects of soil erosion (Atoma et al., 2020). The current investigation practiced the RUSLE model for evaluating sediment yield and soil erosion in the Chitral district consequential of the changes in the land-cover and climate that happened primarily because of the socio-economic growth resulting from the actions of humans and subsequently from global warming. For the estimation of the soil erosion to occur in the future, the RUSLE model is suitable to use by considering the land-cover change model and climate change situations by utilizing the GCMs (Arunyawat & Shrestha, 2016; Azimi Sardari et al., 2019; Plangoen et al., 2013). The GCMs are used for the application of the R factor. They have revised bias along with downscaled grids of spatial resolution of 1 km to analyze the impending rainfall. From the simulation of the LCM with FAO (2000) and Yang et al. (2003), the C and P factors are deliberated correspondingly. As it is not possible to predict two factors relying on space and time, the LS and K factors are established as constant values. For preparing the possible change maps, the LCM model

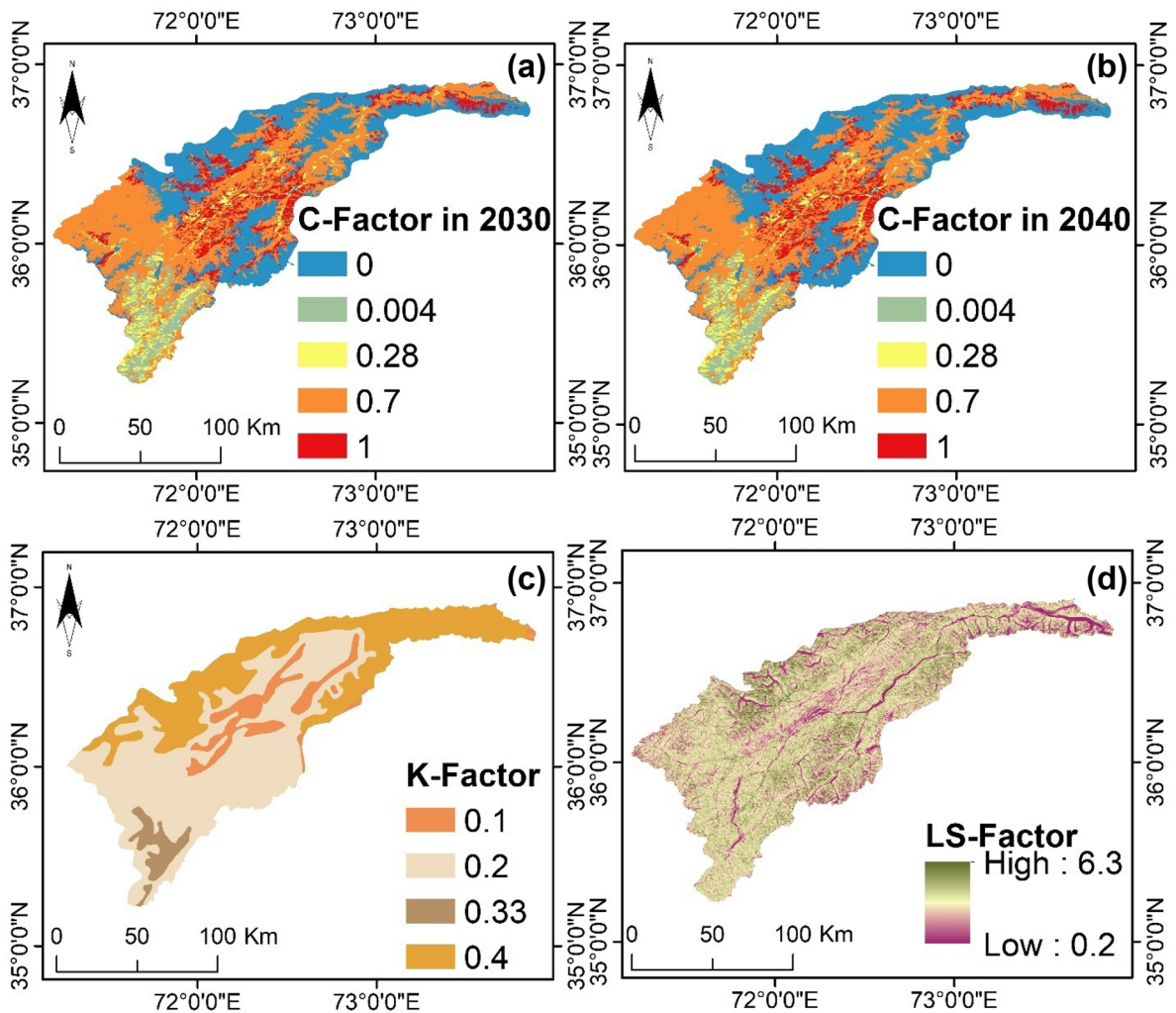


Fig. 7 C factor in 2030 **a** and 2040 **b** and the K factor **c** and LS factor **d** of the study area

is centered on the ANN, whereas it is centered on the Markov chain analysis for the modeling of the possible land-cover maps.

The delta method was used for the downscaling and bias-correcting of the results of rainfall predictions of the MPI-ESM-LR model. The results demonstrated that the tendencies of the rainfalls show an upsurge in magnitude for the future, as shown in Fig. 3. This increase in magnitude can be a result of the effects of change in climate and global warming. The possibility of intense rainfall in some areas will also increase. The outcomes demonstrated the sorts of increased and intense rainfall predictions contrasted to the rainfalls in the historical time during the winter

season, as evident from Fig. 3. Under different RCP scenarios, Eq. (2) was used to calculate the R factor in 2030 and 2040 centered on Aslam et al. (2020). The highest rainfalls, specifically under the RCP4.5 scenario, were excessive compared to the rainfall data of the historical period for all the months. However, the outcomes also exhibited that under the RCP2.6 and RCP8.5 scenarios, the rainfall projections for most months were nearly the same as per the magnitude and highest rainfalls. The dissemination demonstrates a comparable configuration; however, it varies concerning the rainfall magnitude. Earlier research in the study area also specified that the growing rainfall (R factor) because of the change in the climate resulted

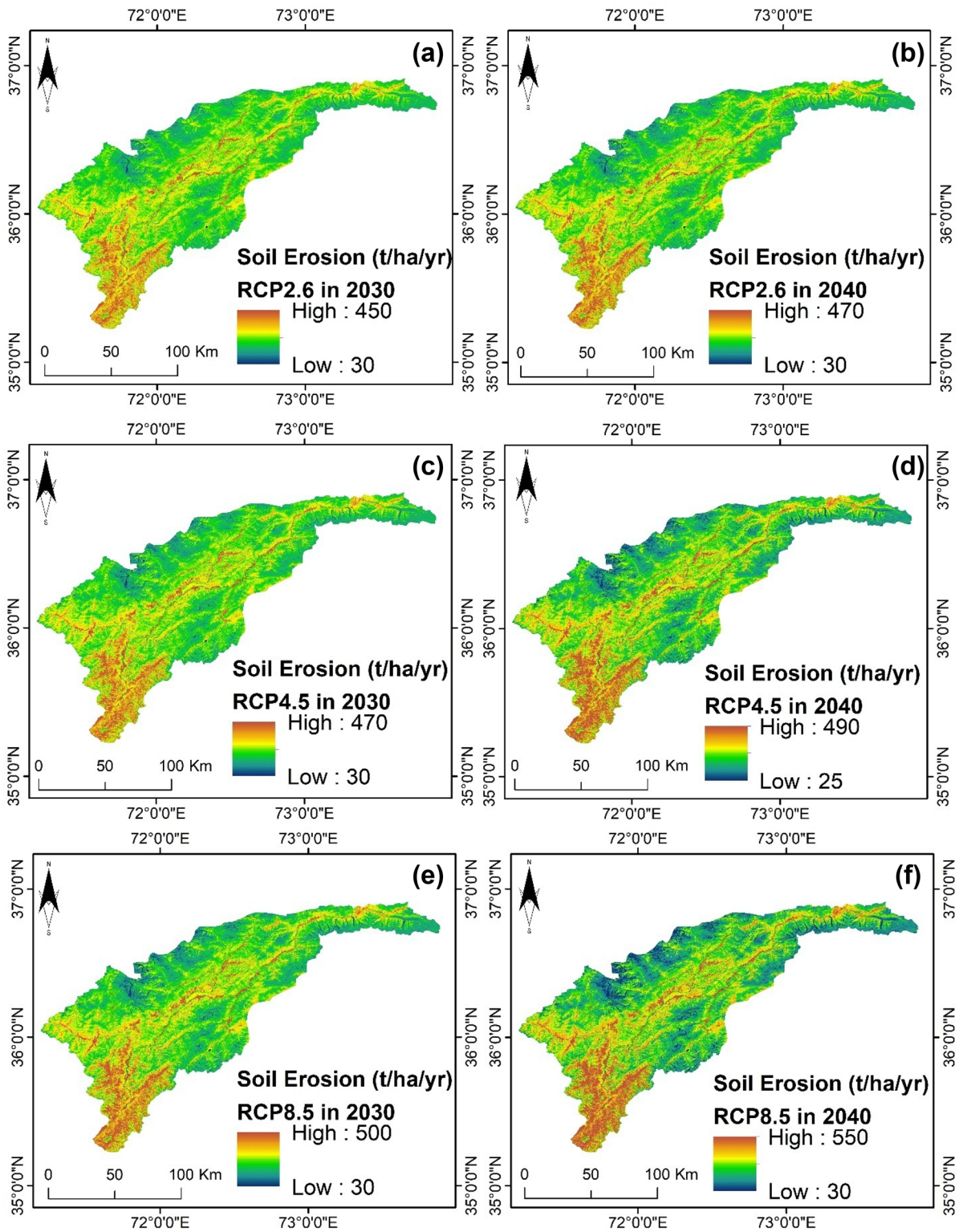


Fig. 8 Soil erosion rate for the study area in 2030 and 2040 under different RCP scenarios

Table 5 Logical outcomes of the correlation among input factors and soil erosion rate

Year	Scenarios	Factors				
		<i>R</i>	<i>K</i>	LS	<i>C</i>	<i>P</i>
2030	RCP2.6	0.214	0.121	0.192	0.424	0.255
	RCP4.5	0.223	0.123	0.199	0.414	0.245
	RCP8.5	0.224	0.124	0.199	0.413	0.245
2040	RCP2.6	0.23	0.107	0.178	0.434	0.255
	RCP4.5	0.229	0.101	0.177	0.433	0.265
	RCP8.5	0.234	0.096	0.172	0.436	0.266

in an increased rate of soil erosion, even though climate circumstances are diverse contingent on each region (Aslam et al., 2020).

The Kappa coefficient was considered to evaluate land-cover maps in 2000, 2010, and 2020. For studying the land-cover change in the Chitral district, the produced land-cover maps can be used as indicated by the precision of the Kappa coefficients. The observed values of the Kappa coefficients were about 0.91, 0.87, and 0.93; thus, these high values were signifying that the precision of the maps was adequate for all the deliberated years. The inclusive precisions of the land-cover maps were found to be 96.4%, 88.3%, and 88.3% by exploiting the general accuracy assessment among the observed and modeled land-cover maps in 2000, 2010, and 2020.

Six descriptive variables, comprising the distance from urban areas, slope, distance from river, distance from roads, aspect, and elevation, were used for the modeling of possible change maps in the LCM module by applying the MLP neural network. The mentioned six descriptive variables were used for producing one land-cover to another, thus defined as six sub-models. Extraordinary accuracy ranging from 71.89 to 86.63% thus reliability was exhibited by all the six sub-models as exhibited in Table 2. Therefore, it can be concluded that in the LCM module, the modeling of possible change by exploiting the MLP neural network is appropriate for the modeling of the land-cover change in the Chitral district.

The possible change maps were used to compute the change prediction process, that is, the possibility of change from one land-cover in 2000 to another in 2020 by utilizing the Markov chain analysis. For studying the change in land-cover, the LCM module in TerrSet software was utilized. The possibility of change matrix from 2000 to 2020 presented in Table 4 was focused for the standardizations of the

land-cover map in 2020 besides the modeling of land-cover projection in 2030 and 2040. According to van Vliet et al. (2011), Plangoen et al. (2013), and Azimi Sardari et al. (2019), four Kappa statistics, namely the K_{standard} , K_{no} , and K_{location} and $K_{\text{location strata}}$, were utilized to assess the accuracy of the cell by using the standardization of the land-cover map in 2020. It can be stated from the results of all the Kappa statistics that the capability of the LCM module in TerrSet software in forecasting the land-cover maps in 2030 as well as 2040 is excellent, and this, in this case, can be due to the use of the Markov chain analysis.

A substantial variation in land-cover from 2000 to 2030 and 2040 was demonstrated by the outcomes (Fig. 5). Most areas were converted to agriculture and build-up and bare areas from the areas composed of natural trees and shrubs as indicated by the results of a comparison among the land-cover maps in 2000, 2030, and 2040 (Table 2). For both in 2030 and 2040, the future land-cover maps specified that the area composed of natural trees mostly decreased by 3% and 4%, and the area composed of natural shrubs decreased approximately by 72,456 and 115,930 ha, correspondingly. From 2000 to 2030 and 2040, the change in agricultural land is continual, and it increases by 6% and 9%, or approximately 86,947 and 130,421 ha. In the district, the socio-economic development resulted in the rapid expansion of the urban area. It expanded from 2000 by 4% and 5% or approximately 149,595 and 101,439 ha. However, the results of land-cover modeling also indicated that the regions covered by snow will transform considerably in the near future because of the effects of climate change in the Chitral district.

DEM having a 30-m spatial resolution was used for the analysis of the LS factor. Nevertheless, the size of the grid size is the coarse spatial resolution that can introduce errors in the exploration of soil

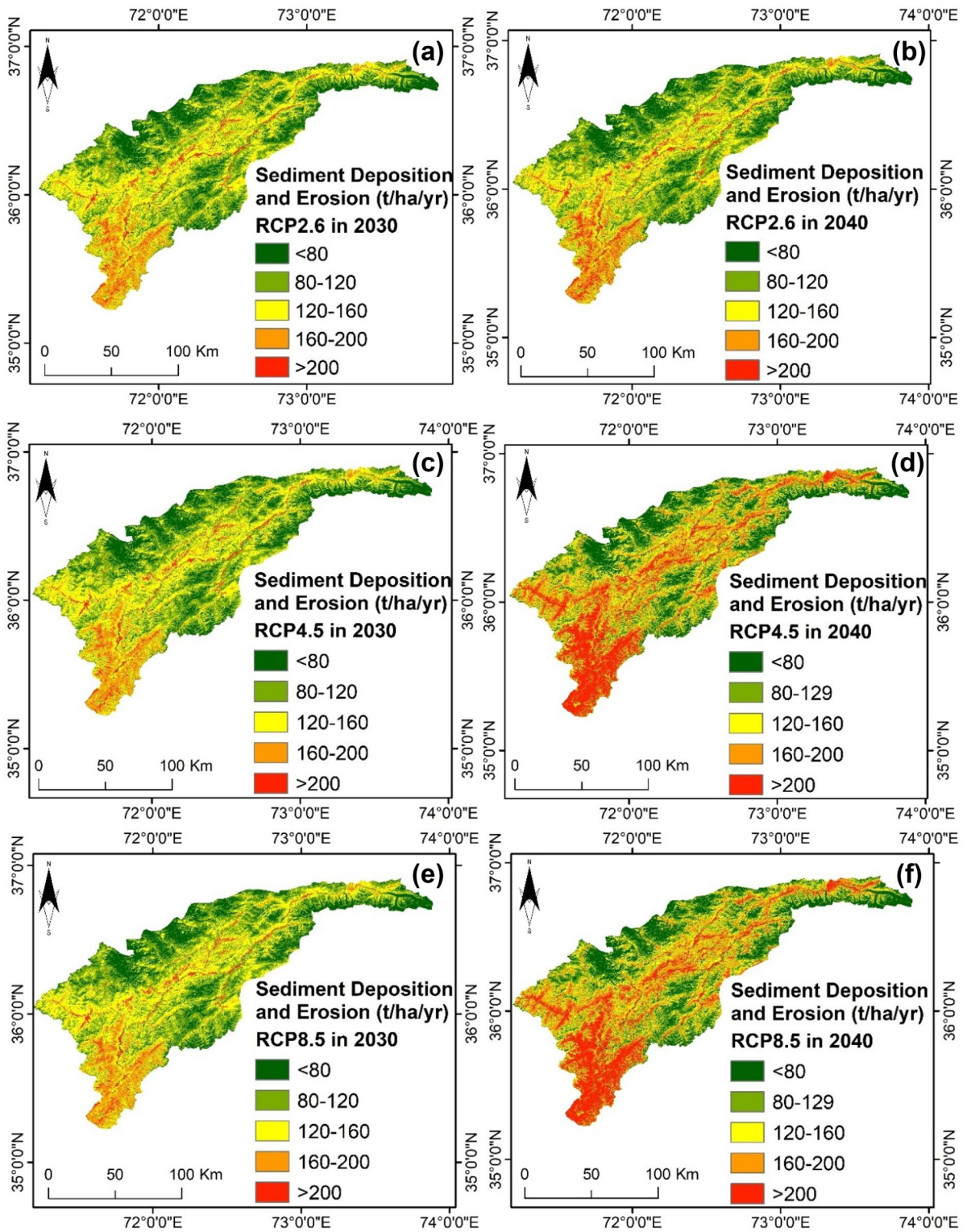


Fig. 9 Sediment deposition and erosion rate for the study area in 2030 and 2040 under different RC

Table 6 Covered area under different severity classes of sediment deposition and erosion in 2030 and 2040 for different RCP scenarios

Sediment deposition and erosion ($t\ ha^{-1}\ yr^{-1}$)	2030						2040					
	RCP2.6		RCP4.5		RCP8.5		RCP2.6		RCP4.5		RCP8.5	
	Area (ha)	Area (%)	Area (ha)	Area (%)	Area (ha)	Area (%)	Area (ha)	Area (%)	Area (ha)	Area (%)	Area (ha)	Area (%)
<80	521,683	36	478,210	33	449,227	31	492,701	34	420,245	29	391,263	27
80–120	362,280	25	318,807	22	333,298	23	347,789	24	289,824	20	275,333	19
120–160	202,877	14	231,859	16	217,368	15	217,368	15	231,859	16	246,351	17
160–200	159,403	11	188,386	13	202,877	14	188,386	13	246,351	17	260,842	18
>200	202,877	14	231,859	16	246,351	17	202,877	14	260,842	18	275,333	19

erosion rates. The upcoming research needs to be vigilant about this concern for further applications. Regardless of the constraints in the field examination of the study area, using the data from FAO (2000) in the LCM module operated in TerrSet software, the values of the C factor were processed. The suggestions by Yang et al. (2003) were followed for specifying the values of the P factor (Table 1). However, for both 2030 and 2040, the range of the P factor was the same as 0.5 to 1. The agricultural area was assigned a P value of 0.5, while for paddy fields, the P values might be smaller than 0.5 in many cases. Thus, we assume that the use of the P factor ought to be contingent on the judgment of the researcher and the fitness of the research. Furthermore, future investigations on soil erosion need to be careful about the arrangement of the P value.

For comparing the soil erosion rate, the study conducted by Aslam et al. (2020) was utilized as a reference for the present research outcomes. The reference study shows that the extreme soil erosion rate was more than 50 t/ha/year from 2000 to 2020. Whereas under different RCP scenarios for future land-cover in 2030 and 2040, our outcomes demonstrated that the soil erosion rate was rising substantially in some of the areas. In 2030 and 2040, the maximum rate of soil erosion was approximately 500 and 550 t/ha/year, correspondingly. The situations of the soil erosion incidence were different as per the pattern from intermediate to high and severe rates and spatial distribution as indicated by the results. Nevertheless, the comparison among the reference (2000 to 2020) and future scenarios in 2030 and 2040 also showed that the minimum rate of soil erosion showed a decline in soil erosion rate for some regions.

Table 5 indicates the correlation analysis outcomes that were performed among the RUSLE input factors and the soil erosion rate by utilizing the SPSS software. In our hypothesis, the extent of statistical significance was stipulated at 95%. As in multiple linear regressions, there is the logarithmic form; for the analysis of the RUSLE input factors besides the soil erosion rate of the Chitral district, the standardized coefficient outcomes can be deemed similar. The specified Eqs. (5–11) can recognize the prominent factors influencing the occurrence intensity of soil erosion.

A few specific regions are converting from areas containing natural trees and shrubs to agricultural and build-up areas in the study area. Because of the great hydropower potential, the study area presents the development and construction of the hydropower projects. Hence, in the near future, the potential change in land-cover is anticipated to lead to the amplified rates of soil erosion. In the Chitral district, the transformation of vegetation cover is among the causes of soil erosion incidence, and these outcomes agreed with those of Aslam et al. (2020). The capability of the C factor can safeguard the topsoil as it protects it from eroding against the eroding agents. Conservation of the land-cover through the enhanced grazing management, reducing the tillage, retention of the crop residue, and cultivating green manure crops and cover crops are among the methods that can be adopted as management choices for soil–water preservation (P factor) in order to lower the vulnerability to nutrient loss and soil erosion. There are also some mitigation co-advantages of the most appropriate options. Nutrient discharge and soil erosion can be reduced by adopting farming systems such as perennial grains, perennial pasture phases, and agro-forestry. For certain soil types and climates, the cover crops have the potential to enhance the soil conditions. Sustainable forest management ways can be employed to cut the degradation of woodlands and deforestation, decreasing greenhouse gas discharges. This mechanism can reduce the extent of forest conservation because these management practices seek to offer biomass, fiber, timber, and non-timber supplies and additional ecosystem services and functions that will reduce greenhouse gas emissions.

Equation (14) was exploited to evaluate the sediment deposition or sediment yield in the Chitral district presented in Fig. 9. The decreasing trend of the area percentage shows that more areas will be subjected to the hazard of sediment deposition and erosion shortly. Similarly, the areas that fall in the very high severity class, despite having less percentage, exhibit an intensifying trend for the future. For the validation of the revised RUSLE model, the obtained outcomes of sediment deposition and erosion were analyzed by exploiting the estimated sediment yield ratio (Y) from the previous two studies in the same district. Under different RCP scenarios both in 2030 and 2040, the outcomes of this study are relatable to the outcomes of Aslam et al. (2020) and Maqsoom

et al. (2020). The outcomes inclusively were satisfactory as per the spatial patterns and trends. The mentioned studies exhibited that the revised RUSLE model can model the Y in the Chitral district. The assessment of the outcomes of observed sediment statistics and the modeled sediment statistics under different RCP scenarios in 2030 and 2040 indicated that they are similar. Under all the RCP scenarios, it can be seen from Fig. 9 that all the modeled results of the Y demonstrated the increasing trends both in 2030 and 2040, particularly in the lower parts of the Chitral district.

The increased sediment in the lower regions of the Chitral district occurred because of the change in land-cover, specifically the conversions of the areas that were covered with natural trees and shrubs to agricultural and build-up lands. The construction of hydropower dams in the region is also somewhat responsible for the increased sediment. The temperature and rainfall circumstances are greatly influenced by the change in climate that, as a result, affects soil erosion and sediments. Moreover, the results of this research specified that in the future, sediment due to the existence of increased soil erosion rate had intensifying tendencies, notably in the center plus the lower regions of the district. In contrast, the peripheral regions had considerably decreasing trends. The lower regions of the study area have been eroding swiftly because of human factors, specifically the variations in the land-cover.

Lower parts of the study area will be experiencing substantial rainfall and swift change in land-cover that have a substantial impact on soil erosion. Changes in the climate because of global warming can result in severe events in this region in the future, for instance, high rainfalls during the wet season, as well as high temperature during the dry season, ensuing certain changes in soil erosion trends and sediments. Therefore, the sediment trends in the study area can be decreased by applying certain soil conservation policies that involve using different measures (either structural or non-structural) coupled with sediment confining of hydropower reservoirs.

The overall results indicated that the Chitral district in the future has been facing defying issues, for instance, population growth, land destruction, and deforestation from advancements in the future as the regions covered by natural trees and shrubs change to build-up regions. In the RUSLE model, the C and P

factors that specify the capacity of vegetation cover, particularly the areas contained by natural trees and shrubs (that safeguard the surface soil from eroding and reduce the impact of possible water erosion), will be affected because of the change in land-cover. Thus, if the area covered by natural trees and shrubs was damaged, then the values of the C factor will grow even though the conversion to agricultural and build-up areas. Therefore, there will be an upsurge in the tendencies of soil erosion rate, and in some of the regions, it may result in extreme erosion.

Conclusion

The present research used the RUSLE model to pursue an investigation that involves evaluating the varying tendencies of soil erosion and sediment yield caused by the potential variations in the land-cover and climate in the Chitral district. The area has a prodigious hydropower potential due to a critical river (Chitral River) that flows through the district. The soil erosion might result in a reduction in the storage level of the reservoirs. It can also have adverse effects on the ecological system and morphology. The C factor, which signifies the cropping as well as management practices in the investigation of soil erosion, is deliberated in terms of the vegetation cover. For the future scenarios, the land-cover change exhibited that most of the areas covered by natural trees and shrubs were transformed into agriculture and build-up areas due to the demands of socio-economic growth in the area. This change increased the C factor. The results of the climate change factor demonstrated an expansion in the mean rainfall of the entire district combined with the highest rainfall rate in some regions. Consequently, in the present research, the values of the R factor for future scenarios exhibited an increase in intensity compared to those in historical times. The outcomes from the anticipated changes in the land-cover and climate scenarios specified an amplified soil erosion rate of 500 and 550 t/ha/year under RCP8.5 in 2030 and 2040, respectively. In most of the lower parts of the Chitral district, the sediment yield was found to be very high (> 200 t/ha/year) under all RCP scenarios in 2030 and 2040. The soil erosion and deposition maps highlight the potentially vulnerable areas. Thus, the outcomes emphasize that the region will be subjected to considerable

soil erosion in the near future. For protecting the soil from eroding, the government authorities need to instantly develop and implement progressive conservation policies in the area by bearing in mind the results of this research. Therefore, to stimulate balanced development and thus regulate the irregular land-cover change, devising and executing the soil–water preservation strategy should be enforced for the deliberated area.

Data availability The datasets generated during and/or analyzed during the current study are available from the corresponding author on reasonable request.

Declarations

Conflict of interests The authors declare no competing interests.

References

- Abdo, H., & Salloum, J. (2017). Mapping the soil loss in Marqya basin: Syria using RUSLE model in GIS and RS techniques. *Environmental Earth Sciences*, 76(3), 114.
- Anand, J., Gosain, A., & Khosa, R. (2018). Prediction of land use changes based on Land Change Modeler and attribution of changes in the water balance of Ganga basin to land use change using the SWAT model. *Science of the Total Environment*, 644, 503–519.
- Ansari, A., & Golabi, M. H. (2019). Prediction of spatial land use changes based on LCM in a GIS environment for Desert Wetlands—A case study: Meighan Wetland. *Iran. International Soil and Water Conservation Research*, 7(1), 64–70.
- Arunyawat, S., & Shrestha, R. P. (2016). Assessing land use change and its impact on ecosystem services in Northern Thailand. *Sustainability*, 8(8), 768.
- Aslam, B., Maqsoom, A., Kazmi, Z. A., Sodangi, M., Anwar, F., Bakri, M. H., & Farooq, D. (2020). Effects of landscape changes on soil erosion in the built environment: Application of geospatial-based RUSLE technique. *Sustainability*, 12(15), 5898.
- Atoma, H., Suryabagavan, K., & Balakrishnan, M. (2020). Soil erosion assessment using RUSLE model and GIS in Huluka watershed. *Central Ethiopia. Sustainable Water Resources Management*, 6(1), 12.
- Azimi Sardari, M. R., Bazrafshan, O., Panagopoulos, T., & Sardooi, E. R. (2019). Modeling the impact of climate change and land use change scenarios on soil erosion at the Minab Dam Watershed. *Sustainability*, 11(12), 3353.
- Chhin, R., & Yoden, S. (2018). Ranking CMIP5 GCMs for model ensemble selection on regional scale: Case study of the Indochina Region. *Journal of Geophysical Research: Atmospheres*, 123(17), 8949–8974.

- Chuenchum, P., Xu, M., & Tang, W. (2020a). Estimation of soil erosion and sediment yield in the Lancang-Mekong river using the modified revised universal soil loss equation and GIS techniques. *Water*, 12(1), 135.
- Chuenchum, P., Xu, M., & Tang, W. (2020b). Predicted trends of soil erosion and sediment yield from future land use and climate change scenarios in the Lancang-Mekong River by using the modified RUSLE model. *International Soil and Water Conservation Research*, 8(3), 213–227.
- Devatha, C., Deshpande, V., & Renukaprasad, M. (2015). Estimation of soil loss using USLE model for Kulhan Watershed, Chattisgarh-A case study. *Aquatic Procedia*, 4, 1429–1436.
- Diyabalanage, S., Samarakoon, K., Adikari, S., & Hewawasam, T. (2017). Impact of soil and water conservation measures on soil erosion rate and sediment yields in a tropical watershed in the Central Highlands of Sri Lanka. *Applied Geography*, 79, 103–114.
- Efthimiou, N., Lykoudi, E., & Karavitis, C. (2014). Soil erosion assessment using the RUSLE model and GIS. *European Water*, 47(15–30), 2014.
- Eroğlu, H., Çakır, G., Sivrikaya, F., & Akay, A. E. (2010). Using high resolution images and elevation data in classifying erosion risks of bare soil areas in the Hatila Valley Natural Protected Area, Turkey. *Stochastic Environmental Research and Risk Assessment*, 24(5), 699–704.
- FAO. (2000). Strategic environmental assessment: An assessment of the impact of cassava production and processing on the environment and biodiversity (Paper presented at the FAO Proceedings of the validation forum on the global cassava development strategy).
- FAO, I. (2015). Status of the world's soil resources (SWSR)—main report. Food and agriculture organization of the United Nations and intergovernmental technical panel on soils, Rome, Italy, 650.
- Ferreira, V., Panagopoulos, T., Andrade, R., Guerrero, C., & Loures, L. (2015). Spatial variability of soil properties and soil erodibility in the Alqueva reservoir watershed. *Solid Earth Sciences*, 6(2), 383–392.
- Fu, B., Zhao, W., Chen, L., Zhang, Q., Lü, Y., Gulinck, H., & Poesen, J. (2005). Assessment of soil erosion at large watershed scale using RUSLE and GIS: A case study in the Loess Plateau of China. *Land Degradation & Development*, 16(1), 73–85.
- Fu, K., & He, D. (2007). Analysis and prediction of sediment trapping efficiencies of the reservoirs in the mainstream of the Lancang River. *Chinese Science Bulletin*, 52(2), 134–140.
- Ganasri, B., & Ramesh, H. (2016). Assessment of soil erosion by RUSLE model using remote sensing and GIS-A case study of Nethravathi Basin. *Geoscience Frontiers*, 7(6), 953–961.
- Gelagay, H. S., & Minala, A. S. (2016). Soil loss estimation using GIS and Remote sensing techniques: A case of Koga watershed, Northwestern Ethiopia. *International Soil and Water Conservation Research*, 4(2), 126–136.
- Giorgetta, M. A., Jungclaus, J., Reick, C. H., Legutke, S., Bader, J., Böttinger, M., & Fieg, K. (2013). Climate and carbon cycle changes from 1850 to 2100 in MPI-ESM simulations for the Coupled Model Intercomparison Project phase 5. *Journal of Advances in Modeling Earth Systems*, 5(3), 572–597.
- Guan, D., Li, H., Inohae, T., Su, W., Nagaie, T., & Hokao, K. (2011). Modeling urban land use change by the integration of cellular automaton and Markov model. *Ecological Modelling*, 222(20–22), 3761–3772.
- Guo, Y., Peng, C., Zhu, Q., Wang, M., Wang, H., Peng, S., & He, H. (2019). Modelling the impacts of climate and land use changes on soil water erosion: Model applications, limitations and future challenges. *Journal of environmental management*, 250, 109403.
- Hoang, L. P., Lauri, H., Kumm, M., Koponen, J., Van Vliet, M. T., Supit, I., & Ludwig, F. (2016). Mekong River flow and hydrological extremes under climate change. *Hydrology and Earth System Sciences*, 20(7), 3027–3041.
- Hua-rong, Y., Zhi-feng, Y., & Bao-shan, C. (2006). Spatial analysis on soil erosion of Lancang River Watershed in Yunnan Province under the support of GIS. *地理研究*, 25(3), 421–429.
- Huang, Y., Wang, F., Li, Y., & Cai, T. (2014). Multi-model ensemble simulation and projection in the climate change in the Mekong River Basin. Part I: temperature. *Environmental monitoring and assessment*, 186(11), 7513–7523.
- Johnson, F., Westra, S., Sharma, A., & Pitman, A. J. (2011). An assessment of GCM skill in simulating persistence across multiple time scales. *Journal of Climate*, 24(14), 3609–3623.
- Kaffas, K., Hrissanthou, V., & Sevastas, S. (2018). Modeling hydromorphological processes in a mountainous basin using a composite mathematical model and ArcSWAT. *CATENA*, 162, 108–129.
- Kamwi, J. M., Cho, M. A., Kaetsch, C., Manda, S. O., Graz, F. P., & Chirwa, P. W. (2018). Assessing the spatial drivers of land use and land cover change in the protected and communal areas of the Zambezi Region. *Namibia. Land*, 7(4), 131.
- Karaburun, A. (2009). Estimating potential erosion risks in Corlu using the GIS based RUSLE method. *Fresenius Environmental Bulletin*, 18(9a), 1692–1700.
- Kayet, N., Pathak, K., Chakrabarty, A., & Sahoo, S. (2018). Evaluation of soil loss estimation using the RUSLE model and SCS-CN method in hillslope mining areas. *International Soil and Water Conservation Research*, 6(1), 31–42.
- Kiem, A. S., Ishidaira, H., Hapuarachchi, H. P., Zhou, M. C., Hirabayashi, Y., & Takeuchi, K. (2008). Future hydroclimatology of the Mekong River basin simulated using the high-resolution Japan Meteorological Agency (JMA) AGCM. *Hydrological Processes: An International Journal*, 22(9), 1382–1394.
- Licznar, P. (2004). Prognozowanie erozyjności deszczy w Polsce na podstawie miesięcznych sum opadów. *Archiwum Ochrony Środowiska*, 30(4), 29–39.
- Lufafa, A., Tenywa, M., Isabirye, M., Majaliwa, M., & Woome, P. (2003). Prediction of soil erosion in a Lake Victoria basin catchment using a GIS-based Universal Soil Loss model. *Agricultural Systems*, 76(3), 883–894.
- Mandle, L., Wolny, S., Bhagabati, N., Helsing, H., Hamel, P., Bartlett, R., & Manley, D. (2017). Assessing ecosystem service provision under climate change to support conservation and development planning in Myanmar. *PLoS one*, 12(9), e0184951.

- Maqsoom, A., Aslam, B., Hassan, U., Kazmi, Z. A., Sodangi, M., Tufail, R. F., & Farooq, D. (2020). Geospatial assessment of soil erosion intensity and sediment yield using the revised universal soil loss equation (RUSLE) model. *ISPRS International Journal of Geo-Information*, 9(6), 356.
- Mas, J.-F., Kolb, M., Paegelow, M., Olmedo, M. T. C., & Houet, T. (2014). Inductive pattern-based land use/cover change models: A comparison of four software packages. *Environmental Modelling & Software*, 51, 94–111.
- Mehran, A., AghaKouchak, A., & Phillips, T. J. (2014). Evaluation of CMIP5 continental precipitation simulations relative to satellite-based gauge-adjusted observations. *Journal of Geophysical Research: Atmospheres*, 119(4), 1695–1707.
- Mitasova, H., Mitas, L., Brown, W. M., & Johnston, D. M. (1999). *Terrain modeling and soil erosion simulations for Fort Hood and Fort Polk test areas*. University of Illinois at Urbana-Champaign.
- Moss, R. H., Edmonds, J. A., Hibbard, K. A., Manning, M. R., Rose, S. K., Van Vuuren, D. P., & Kram, T. (2010). The next generation of scenarios for climate change research and assessment. *Nature*, 463(7282), 747–756.
- Navarro-Racines, C., Tarapues, J., Thornton, P., Jarvis, A., & Ramirez-Villegas, J. (2020). High-resolution and bias-corrected CMIP5 projections for climate change impact assessments. *Scientific Data*, 7(1), 1–14.
- Navarro-Racines, C. E., & Tarapues, J. (2015). Bias-correction in the CCAFS-Climate Portal: A description of methodologies.
- Nor, A. N. M., Corstanje, R., Harris, J. A., & Brewer, T. (2017). Impact of rapid urban expansion on green space structure. *Ecological Indicators*, 81, 274–284.
- Nord, G., & Esteves, M. (2005). PSEM_2D: A physically based model of erosion processes at the plot scale. *Water resources research*, 41(8).
- Norris, J. R. (1998). *Markov chains*: Cambridge university press.
- Olmedo, M. T. C., Pontius, R. G. Jr., Paegelow, M., & Mas, J.-F. (2015). Comparison of simulation models in terms of quantity and allocation of land change. *Environmental Modelling & Software*, 69, 214–221.
- Ozcan, A. U., Erpul, G., Basaran, M., & Erdogan, H. E. (2008). Use of USLE/GIS technology integrated with geostatistics to assess soil erosion risk in different land uses of Indagi Mountain Pass—Cankırı. *Turkey. Environmental Geology*, 53(8), 1731–1741.
- Peng, J., Li, D., & Zhang, Y. (2007). Analysis of spatial characteristics of soil erosion in mountain areas of northwestern Yunnan based on GIS and RUSLE. *Journal of Mountain Science*, 25(5), 548–556.
- Pérez-Vega, A., Mas, J.-F., & Ligmann-Zielinska, A. (2012). Comparing two approaches to land use/cover change modeling and their implications for the assessment of biodiversity loss in a deciduous tropical forest. *Environmental Modelling & Software*, 29(1), 11–23.
- Plangoen, P., Babel, M. S., Clemente, R. S., Shrestha, S., & Tripathi, N. K. (2013). Simulating the impact of future land use and climate change on soil erosion and deposition in the Mae Nam Nan sub-catchment. *Thailand. Sustainability*, 5(8), 3244–3274.
- Polykretis, C., Alexakis, D. D., Grillakis, M. G., & Manoudakis, S. (2020). Assessment of intra-annual and inter-annual variabilities of soil erosion in Crete Island (Greece) by incorporating the Dynamic “Nature” of R and C-Factors in RUSLE modeling. *Remote Sensing*, 12(15), 2439.
- Raghavan, S. V., Liu, J., Nguyen, N. S., Vu, M. T., & Liang, S.-Y. (2018). Assessment of CMIP5 historical simulations of rainfall over Southeast Asia. *Theoretical and Applied Climatology*, 132(3–4), 989–1002.
- Rahman, M. R., Shi, Z., & Chongfa, C. (2009). Soil erosion hazard evaluation—An integrated use of remote sensing, GIS and statistical approaches with biophysical parameters towards management strategies. *Ecological Modelling*, 220(13–14), 1724–1734.
- Ramirez-Villegas, J., & Jarvis, A. (2010). Downscaling global circulation model outputs: The delta method decision and policy analysis Working Paper No. 1. *Policy Analysis*, 1, 1–18.
- Rangsiwanichpong, P., Kazama, S., & Gunawardhana, L. (2018). Assessment of sediment yield in Thailand using revised universal soil loss equation and geographic information system techniques. *River Research and Applications*, 34(9), 1113–1122.
- Renard, K., Foster, G., & Weesies, G. (1997). Predicting soil erosion by water: a guide to conservation planning with the Revised Universal Soil Loss Equation (RUSLE). *Agriculture handbook* (703).
- Ricker, M. C., Odhiambo, B. K., & Church, J. M. (2008). Spatial analysis of soil erosion and sediment fluxes: A paired watershed study of two Rappahannock River tributaries, Stafford County. *Virginia. Environmental Management*, 41(5), 766–778.
- Ruan, Y., Liu, Z., Wang, R., & Yao, Z. (2019). Assessing the performance of CMIP5 GCMs for projection of future temperature change over the lower Mekong Basin. *Atmosphere*, 10(2), 93.
- Ruangrassamee, P., Khamkong, A., & Chuenchum, P. (2015). Assessment of precipitation simulations from CMIP5 climate models in Thailand. Paper presented at the The 3rd EIT International Conference on water Resource Engineering.
- Rumelhart, D. E., Hinton, G. E., & Williams, R. J. (1985). *Learning internal representations by error propagation*. California Univ San Diego La Jolla Inst for Cognitive Science.
- Schuol, J., Abbaspour, K. C., Srinivasan, R., & Yang, H. (2008). Estimation of freshwater availability in the West African sub-continent using the SWAT hydrologic model. *Journal of Hydrology*, 352(1–2), 30–49.
- Sharma, A., Tiwari, K. N., & Bhadoria, P. (2011). Effect of land use land cover change on soil erosion potential in an agricultural watershed. *Environmental Monitoring and Assessment*, 173(1–4), 789–801.
- Singh, G., & Panda, R. K. (2017). Grid-cell based assessment of soil erosion potential for identification of critical erosion prone areas using USLE, GIS and remote sensing: A case study in the Kapgari watershed, India. *International Soil and Water Conservation Research*, 5(3), 202–211.
- Tangang, F., Santisirisomboon, J., Juneng, L., Salimun, E., Chung, J., Supari, S., & Singhruck, P. (2019). Projected future changes in mean precipitation over Thailand based on multi-model regional climate simulations of CORDEX Southeast Asia. *International Journal of Climatology*, 39(14), 5413–5436.

- Taylor, K. E., Stouffer, R. J., & Meehl, G. A. (2012). An overview of CMIP5 and the experiment design. *Bulletin of the American Meteorological Society*, 93(4), 485–498.
- Teng, H., Liang, Z., Chen, S., Liu, Y., Rossel, R. A. V., Chappell, A., & Shi, Z. (2018). Current and future assessments of soil erosion by water on the Tibetan Plateau based on RUSLE and CMIP5 climate models. *Science of the Total Environment*, 635, 673–686.
- Terranova, O., Antronico, L., Coscarelli, R., & Iaquina, P. (2009). Soil erosion risk scenarios in the Mediterranean environment using RUSLE and GIS: An application model for Calabria (southern Italy). *Geomorphology*, 112(3–4), 228–245.
- Thuy, H. T., & Lee, G. (2017). Soil loss vulnerability assessment in the Mekong River Basin. *한국지반환경공학회 논문집*, 18(1), 37–47.
- Ullah, S., Ali, A., Iqbal, M., Javid, M., & Imran, M. (2018). Geospatial assessment of soil erosion intensity and sediment yield: A case study of Potohar Region. *Pakistan. Environmental Earth Sciences*, 77(19), 705.
- Vaezi, A. R., Abbasi, M., Keesstra, S., & Cerdà, A. (2017). Assessment of soil particle erodibility and sediment trapping using check dams in small semi-arid catchments. *CATENA*, 157, 227–240.
- van Vliet, J., Bregt, A. K., & Hagen-Zanker, A. (2011). Revisiting Kappa to account for change in the accuracy assessment of land-use change models. *Ecological Modelling*, 222(8), 1367–1375.
- Verburg, P. H., Soepboer, W., Veldkamp, A., Limpiada, R., Espaldon, V., & Mastura, S. S. (2002). Modeling the spatial dynamics of regional land use: The CLUE-S model. *Environmental Management*, 30(3), 391–405.
- Wijesundara, N., Abeysingha, N., & Dissanayake, D. (2018). GIS-based soil loss estimation using RUSLE model: A case of Kirindi Oya river basin, Sri Lanka. *Modeling Earth Systems and Environment*, 4(1), 251–262.
- Wischmeier, W. H., & Smith, D. D. (1978). Predicting rainfall erosion losses: A guide to conservation planning: Department of Agriculture, Science and Education Administration.
- Yang, D., Kanae, S., Oki, T., Koike, T., & Musiak, K. (2003). Global potential soil erosion with reference to land use and climate changes. *Hydrological Processes*, 17(14), 2913–2928.
- Yao, H., Yang, Z., & Cui, B. (2005). Soil erosion and its environmental background at Lancang Basin of Yunnan Province. *Bulletin of Soil and Water Conservation*, 25, 5–14.
- Zhou, Q., Yang, S., Zhao, C., Cai, M., & Ya, L. (2014). A soil erosion assessment of the upper Mekong River in Yunnan Province. *China. Mountain Research and Development*, 34(1), 36–47.

Publisher's Note Springer Nature remains neutral with regard to jurisdictional claims in published maps and institutional affiliations.